Earth System
Dynamics

Open Access

Discussions

EGU

Annual and semiannual cycles of midlatitude surface temperature and baroclinicity: reanalysis data and AOGCMs simulations

Valerio Lembo[1], Isabella Bordi[2,3], Antonio Speranza[2]

[1]Department of Biological and Environmental Sciences and Technologies (DiSTeBA), University of Salento, Lecce, Italy
5   [2]National Interuniversity Consortium for the Physics of the Atmosphere and Hydrosphere (CINFAI), Rome, Italy
[3]Department of Physics, Sapienza University of Rome, Rome, Italy

Correspondence to: Isabella Bordi (isabella.bordi@cinfai.it), Valerio Lembo (valerio.lembo@unisalento.it)

Abstract. Seasonal variability of surface air temperature and baroclinicity from the ECMWF ERA-Interim (ERAI) reanalysis and six coupled atmosphere-ocean general circulation models (AOGCMs) participating in the Coupled Model
10   Intercomparison Project phase 3 and 5 (CMIP3 and CMIP5) are examined. In particular, the annual and semiannual cycles of hemispherically averaged fields are studied using spectral analysis. The aim is to assess the ability of coupled general circulation models to properly reproduce the observed amplitude and phase of these cycles, and investigate the relationship between surface temperature and baroclinicity (coherency and relative phase) in such frequency bands. The overall results of power spectra agree in displaying a statistically significant peak at the annual frequency in the zonally averaged fields of
15   both hemispheres. The semiannual peak, instead, shows less power and in the NH seems to have a more regional character, as is observed in the North Pacific Ocean region. Results of bivariate analysis for such a region and Southern Hemisphere midlatitudes show some discrepancies between ERAI and model data, as well as among models, especially for the semiannual frequency. Specifically: (i) the coherency at the annual and semiannual frequency observed in the reanalysis data is well represented by models in both hemispheres; (ii) at the annual frequency, estimates of the relative phase between
20   surface temperature and baroclinicity are bounded between about $\pm 15^{o}$ around an average value of 220° (i.e., approximately 1 month phase shift), while at the semiannual frequency model phases show a wider dispersion in both hemispheres with larger errors in the estimates, denoting increased uncertainty and some disagreement among models. The most recent CMIP climate models (CMIP5) show several improvements when compared with CMIP3 but a degree of discrepancy still persists though masked by the large errors characterizing the semiannual frequency. These findings contribute to better characterize
25   the cyclic response of current global atmosphere-ocean models to the external (solar) forcing that is of interest for seasonal forecasts.

1 Introduction

The seasonal cycle of the heating of the atmosphere to which contributes mostly the upward energy fluxes from the surface (i.e., longwave, latent and sensible heat fluxes) and to a lesser extent the direct shortwave absorption, is one of the most prominent features of the Earth's climate (e.g., Kiehl and Trenberth, 1997; Trenberth and Stepaniak, 2004). A recent study

5   by Donohoe and Battisti (2013) suggested that while the annual average heating is dominated by upward energy fluxes from the surface, most of the seasonal heating is due to the shortwave absorption within the atmosphere that is quite constant throughout the troposphere. This would be explained by the fact that in the annual cycle the insolation transmitted to the surface goes primarily into storage (especially over the ocean) and the atmosphere is heated from below. It is estimated that the variation of solar insolation, due to the orbital movement of the Earth around the Sun, accounts for about 90 % of the

10   total variance of surface temperature (Trenberth, 1983).

Observations show that at midlatitudes the annual harmonic is by far the largest component of the seasonal cycle, while other sub-harmonics capture only the finer structure of the cyclic variation. Approaching the equatorial regions, the seasonal cycle has a more complicated behavior and the annual and semiannual harmonics are both large components. The semiannual signal characterizes also high-latitude regions. Furthermore, there are observed differences in the seasonality of atmospheric

15   temperature and eddy activity between the Northern and Southern Hemispheres (hereafter NH and SH), with the NH exhibiting stronger seasonal variation due to the larger portion of land surface (Peixoto and Oort, 1992).

Since the first efforts on the climate impact of increasing atmospheric carbon dioxide (Hansen et al., 1981), surface temperature is taken as a proxy in climate change studies. Moreover, due to its decorrelation length (about 1200 km; Hansen and Lebedeff, 1987) and the key role in radiative transfer, it is considered a useful variable for studying large-scale processes

20   and climate sensitivity. Large-scale seasonal variability of surface temperature has been successfully simulated in earlier energy balance models (EBMs), with "passive" ocean and atmospheric heat transports parameterized as a diffusive process (e.g., North et al., 1983; Kim and North, 1992). The simulation of the seasonal cycle of near-surface air temperature has long been considered a test of performance of climate models (Covey et al., 2000). The ability of coupled General Circulation Models (GCMs) to simulate a reasonable seasonal cycle is, in fact, a necessary condition for confidence in their prediction of

25   long-term climatic behavior, including global changes (e.g., Bye et al., 2013). Furthermore, the amplitude of the seasonal cycle in surface temperature has been used to verify the climate sensitivity of models (Lindzen et al., 1995; Knutti et al., 2006), and the magnitude of the seasonal cycle has been found to be a good predictor of the magnitude of decadal variability in regional surface temperatures (Huybers and Curry, 2006).

The seasonal cycle is also the main modulator of weather variability at midlatitudes. It is well known that transient eddies,

30   which transport heat and momentum in the extratropics, are generated by the horizontal temperature gradient in the mean flow through a process of energy conversion from available potential to kinetic. Such a temperature gradient (often referred to as baroclinicity) is the basis for eddies' development in linear instability theories, nonlinear models of geostrophic turbulence, and observations (e.g., Lindzen and Farrell, 1980; Held and Larichev, 1996; Hoskins and Valdes, 1990). Several

analyses have pointed out that there are regions of enhanced eddy activity, where weather systems preferentially grow through baroclinic instability and subsequently decay, which are referred to as storm tracks. In NH, such regions lie downstream, and slightly poleward, of the cores of the jet stream over the North Atlantic and Pacific Oceans (e.g., Blackmon et al., 1977). It has also been shown that, like most of atmospheric processes, baroclinic activity is characterized by a

5   seasonal cycle. Previous studies, in fact, provided evidences for some kind of midwinter suppression of baroclinic wave activity in the NH Pacific, with large variances during spring and autumn (see Nakamura 1992 and references therein). This finding was supported by the harmonic analysis of air temperature and sea level pressure fields carried out by Yashyayaev and Zveryaev (2001), by observations as illustrated by Chang (2003), or the recent study by Chen et al. (2012).

In SH midlatitudes, an important signature of the seasonal cycle is the Southern Hemisphere Semiannual Oscillation (SAO),

10   a coupled ocean-atmosphere phenomenon that involves the different annual cycles of temperature between the Antarctic polar continent and the surroundings midlatitude oceans (van Loon, 1967; Meehl, 1991). The twice-yearly intensification of temperature gradient between midlatitudes (ocean dominated) and polar latitudes (continental) is associated with a fluctuation in the storm activity.

The persistent character of these regional features in both hemispheres suggests that some processes are acting on the system

15   to self-sustain the storm tracks, i.e. external forcing and/or feedback mechanisms. Thus, investigating the possible relationship between baroclinicity and surface temperature seasonal cycles may help to better understand the role played by the latter (which is directly related to solar forcing and heat fluxes) in modulating the atmospheric processes at midlatitudes. Following Lorenz (1979), variations of weather and climate are forced or free according to whether they result from changes in the external conditions or not. Such a characterization is usually analyzed by examining the correlation between two

20   variables of interest, for example the eddy heat fluxes and baroclinicity (e.g., Stone et al., 1982).

In the present paper, the annual and semiannual harmonics of midlatitude surface temperature and baroclinicity in both hemispheres are studied by applying spectral analysis to ERA-Interim reanalysis and Coupled Model Intercomparison Project (CMIP) data. Furthermore, the relationship (coherency and relative phase) between surface temperature and baroclinicity, which is here estimated using the maximum Eady growth rate, is investigated. The aim is to assess the ability

25   of coupled atmosphere-ocean general circulation models (AOGCMs) to properly reproduce the amplitude and phase of the observed annual and semiannual periodicities that are of interest for seasonal forecasts.

The structure of the paper is as follows. Section 2 describes data and methods, while Section 3 provides a description of the main results obtained from spectral analysis. A summary and conclusions are given in the final section.

2 Data and methods

2.1 Data

Data used for the study are derived from (i) the ERA-Interim archive and (ii) the Coupled Model Intercomparison Project phase 3 (CMIP3) multi-model dataset, including the most recent phase 5 of the project (CMIP5) for comparison.

Earth System
Dynamics
Discussions

ERA-Interim (hereafter ERAI) is the latest global atmospheric reanalysis product delivered by the European Centre for Medium Range Weather Forecasts (ECMWF; Berrisford et al., 2011). The data assimilation system used to produce ERAI is based on the 2006 release of the Integrated Forecasting System (IFS) that includes a 4-dimensional variational analysis (4D-Var) with a 12-hour analysis cycle. In each cycle, all available observations (in situ measurements, radiosondes, satellites, etc.) are combined with prior information from the forecast model to estimate the evolving state of the atmosphere (Dee et al., 2011). The model has T255 horizontal spectral resolution (~ 80 km) with 60 vertical levels from the surface up to 0.1 hPa. ERAI improved on several deficiencies reported in the previous reanalysis ERA-40, in particular the water cycle that was too wet in the tropics and breaks in the time series of some products that are likely related to the introduction of satellites into the assimilation scheme (Poli et al., 2010).

In the present study, monthly means of daily means of 2-meter temperature (T2m) and tropospheric temperature (T) covering the period January 1979–September 2015, at 1-degree horizontal resolution and 8 vertical levels in the troposphere (from 1000 hPa to 300 hPa), are considered and analyzed.

Under the World Climate Research Programme (WCRP), the Working Group on Coupled Modelling (WGCM) established the CMIP as a standard experimental protocol for studying the outputs of coupled AOGCMs. The phase 3 multi-model dataset is here used: it accounts for historical climate reconstruction performed by models, from the pre-industrial era to the beginning of the 21st century (Meehl et al., 2007). The integration period, the radiative forcing parameterization and the horizontal resolution vary from model to model. Whatever is the model vertical resolution, a minimum number of pressure levels for vertical discretization of 3D atmospheric outputs is required to be 17 specified levels from 1000 to 10 hPa. For the present analysis 8 pressure levels from 1000 to 300 hPa are considered (see for details http://www-pcmdi.llnl.gov/ipcc/model_documentation/ipcc_model_documentation.php).

Based on the intraseasonal and interannual variability analysis at milatitudes carried out by Lucarini et al. (2007), for the purpose of the present study, a subset of 6 models over 27 were chosen (see Table 1). The selection has been made taking into account models' performance, when compared with reanalyses, and the horizontal resolution. For CMIP3, the subset comprises one high-resolution model (MIROC3.2), four medium-resolution models (CGCM3.1, ECHAM5/MPI-OM, FGOALS-g1.0, GFDL-CM2.1) and one coarse resolution model (INM-CM3.0). According to Lucarini et al. (2007), while CGCM3.1, GFDL-CM2.1 and MIROC3.2 high-resolution compare well with the reanalysis, ECHAM5/MPI-OM and FGOALS-g1.0 have been found to overestimate both intraseasonal and interannual variability. INM-CM3.0 is here considered as an example of a coarse-resolution model.

Aiming to verify any improvement in the model representation of the features of interest, the most recent multi-model dataset CMIP5 has been also considered (Taylor et al., 2012; http://cmip-pcmdi.llnl.gov/cmip5/guide_to_cmip5.html). CMIP5 differs from earlier phases in the wider variety of scientific issues to be addressed, the larger number of models participating into the project, the generally higher spatial model resolution, a richer set of output fields archived, and the two time scales of the experiments (i.e., long-term and near-term decadal prediction runs). For the present analysis, 6 CMIP5 models, which represent the updated versions of the ones described above, have been selected (see Table 1). It is worth

Earth System Dynamics

Discussions

Open Access

noticing that, in the new ensemble dataset (CMIP5), the model ECHAM5/MPI-OM (CMIP3) has been replaced by MPI-ESM-MR, which is the ECHAM6 model coupled with the same ocean model MPIOM used in phase 3. Furthermore, INM-CM4 and MIROC5 horizontal resolutions are close to those of the medium-resolution CMIP3 models. As for CMIP3, the same 17 vertical pressure levels are required for the atmospheric outputs and 8 levels (up to 300 hPa) have been considered

5   for the representation of the tropospheric mean conditions.

2.2 Methods

Baroclinicity

Synoptic eddy activity in midlatitudes has long been related to the baroclinic instability that converts available potential energy of the time mean flow to eddy kinetic energy (e.g., Charney, 1947; Eady, 1949; Lorenz, 1955). One of the measures

10   of atmospheric baroclinicity is the maximum growth rate of the linear Eady model, which has been shown to be a useful estimate of the growth rate of the most rapidly growing instability in a wide range of baroclinic instability problems (Lindzen and Farrell, 1980). The maximum Eady growth rate has been found to be a suitable parameter to quantify the geographical location and intensity of the storm tracks (i.e., Hoskins and Valdes, 1990; Wu et al., 2011), to evaluate the impact of increasing greenhouse gases and sulphate aerosols on extratropical cyclone activity (Carnell and Senior, 1998;

15   Geng and Sugi, 2003), and to measure the baroclinicity of the mean state of the atmosphere (e.g., Heo et al., 2012). In the present paper, it is applied to the reanalysis and model data. Making use of the thermal wind equation, an accurate estimate of the dimensional growth rate (hereafter referred to as baroclinicity index) is given by (Lindzen and Farrell, 1980):

$$\sigma_{BI} = 0.3125 \frac{f}{N} \left| \frac{\partial \bar{U}}{\partial z} \right| \approx -0.3125 \frac{g}{a\bar{T}N} \left| \frac{\partial \bar{T}}{\partial \phi} \right| \tag{1}$$

20

with f the Coriolis parameter, U the horizontal wind vector, a the Earth's radius, ϕ the latitude, g the gravity acceleration, $\bar{T}$ the mean temperature in the troposphere and N the Brunt-Väisälä frequency, a measure of the static stability. As can be noted, the dry Eady growth rate (moist processes generally lead to an increase of the rate; see Emanuel et al., 1987) is affected by changes of both meridional temperature gradient (or vertical wind shear) and static stability. However, in the

25   present study, N is taken to be constant and equal to the mean tropospheric value of $1.2 \cdot 10^{-2}$ s^{-1} (Holton, 2004). The average over both hemispheres here considered, in fact, cuts off most of the variability of the Brunt-Väisälä frequency that occurs mainly near the surface and at high latitudes (Simmons and Hoskins, 1980).

As introduced in the previous section, surface temperature is taken as the air temperature at 2 meters height, while tropospheric temperature takes into account the 8 pressure levels between 1000 and 300 hPa for both ERAI and AOGCMs.

30   Both fields, surface temperature and tropospheric temperature, are separately considered for the NH and SH. In NH, baroclinicity index is computed over the latitude band 30°–60°N, the area of most intense baroclinic activity (Dell'Aquila et

al., 2007a); in SH, the latitude band 30°–70°S is considered where the bulk of baroclinic and low-frequency planetary waves activity is observed (Dell'Aquila et al., 2007b). The meridional temperature gradient in (1) is computed as the difference between the two boundaries of the considered midlatitude belt, while vertical average of tropospheric temperature is obtained without weighting for the air mass.

5

Spectral analysis

The spectral components of surface air temperature and baroclinicity have been estimated and tested for statistical significance by using the Multi Taper Method (MTM), which is a nonparametric technique widely applied to problems in the analysis of geophysical signals (Thomson, 1982; Percival and Walden, 1993). MTM attempts to reduce the variance of

10 spectral estimates by using a small set of tapers (or spectral windows) rather than single data taper used by other methods like Blackman-Tukey. Data are pre-multiplied by orthogonal tapers (or eigentapers), which are constructed to minimize the spectral leakage due to the finite length of the data series, and, by performing a Fourier Transform, a set of independent power spectral density (PSD) estimates is computed. The optimal tapers belong to a family of functions known as Discrete Prolate Spheroidal Sequences (DPSS) or Slepian sequences, which solve the variational problem of minimizing leakage

15 outside of a frequency band of half bandwidth pf_n, where $f_n = 1/(N \Delta t)$ is the Rayleigh frequency (i.e., the minimum frequency that can be resolved by a finite duration time window), Δt the sampling time, and p an integer. Typically, the number of tapers used K should be less than $(2p-1)$, i.e. the minimum number of tapers that provide small spectral leakage (Ghil et al., 2002). Thus, the bandwidth $2pf_n$ and the number of tapers K represent the key parameters for the stability of the power spectral estimate, which become:

20

$$S = \frac{1}{K} \sum_{k=1}^{K} \Delta t \left| \sum_{t=1}^{N} DPSS_{t,k} \, x(t) e^{-i2\pi f \Delta t} \right|^2 \qquad (2)$$

where $x(t)$ denotes the signal, $DPSS_{t,k}$ is the kth taper function at time point t.

The confidence intervals in the PSD estimates are computed using the chi-squared approach at the 97.5 % confidence level.

25 To investigate the relation between the two fields of interest (surface temperature and baroclinicity) in the frequency domain, the bivariate spectral analysis is performed. The relationship between two time series in the Fourier domain can be expressed in terms of the cross-spectrum, the phase difference, and the cross-coherence, which is defined as follows.

Being $P_A(f)$ and $P_B(f)$ be the complex Fourier spectra of two time series, the cross-spectrum is defined as:

30 $$P_{AB} = P_A(f) \cdot P_B^*(f) \qquad (3)$$

with the asterisk denoting the conjugate. The phase difference can be written as:

6

$$\Phi_{AB}(f) = \arg \langle P_{AB}(f) \rangle \tag{4}$$

with the convention that a value between 0° and 180° means that *A* leads *B* (in our case T2m leads σ_{BI}) and vice versa for a
5   value between 180° and 360°.

The coherence spectrum is a measure of the correlation of the two spectra as a function of frequency and can be written as:

$$COH_{AB}(f) = \frac{\left| \langle P_{AB}(f) \rangle \right|}{\sqrt{\langle |P_A(f)|^2 \rangle \langle |P_B(f)|^2 \rangle}} \tag{5}$$

10   The angle brackets denote the expectation value and can be approximated by a mean over many short spectra (Von Storch
and Zwiers, 1999).

3 Results

To provide a frame of reference for the subsequent analysis, we first present the time series of midlatitude surface
temperature and baroclinicity in both hemispheres as derived by ERAI reanalysis. The seasonal behavior of some averaged
15   fields (i.e., TOA solar radiation, mean sea level pressure, and meridional gradient of geopotential height field at 300 hPa and
500 hPa) introduce and complement this preliminary analysis.

For illustrative purposes, the spectral analysis for selected CMIP3 coupled models follows; results for both hemispheres are
illustrated and compared with those from the most recent CMIP5 models.

3.1 Time series analysis

20   In Figure 1 the observed seasonal variability in both hemispheres of ERAI surface temperature and baroclinicity are
displayed with that of solar radiation at TOA, the meridional gradient (defined as the difference between 30° and 70°) of the
geopotential height (GPT) field at 300 hPa and 500 hPa, and the mean sea level pressure (MSLP) variance in the midlatitude
belt. The annual mean cycles have been computed by averaging daily values over the entire time record of the reanalysis data
and applying 15-day moving average to filter out the high-frequency variability; then, they have been standardized for
25   comparison. For illustrative purposes, the baroclinicity, GPT, and MSLP variance cycles have been reversed so that their
maxima occur in summer as for the other fields.

From Figure 1a (NH) it can be noted that, moving from January to December, the incoming solar radiation precedes the
other signals: in particular, it is followed by surface temperature and baroclinicity index. The meridional geopotential

gradient at 300 hPa and 500 hPa appears in phase with the baroclinicity index, while surface temperature shows a delay of 30–45 days with respect to the incoming solar radiation, and of about 20 days with respect to baroclinicity and geopotential gradients. The annual cycles for the SH (Figure 1b) show similar features with a more pronounced semiannual oscillation in the geopotential gradient and baroclinicity index. A hint of SAO is also observed in MSLP variance cycle. Furthermore, the

5   standardization allows estimating the relative amplitude of the annual cycles that can be grouped as: on one hand, surface temperature and MSLP variance, and on the other hand, meridional geopotential gradients and baroclinicity index.

Monthly mean time series (1979–2015) of both ERAI surface temperature and baroclinicity averaged over the NH and SH midlatitude belts are shown in Figure 2 and 3, respectively. Figures clearly show that the periodic components account for most of the variability of the time series: the annual cycle characterizes the time series with larger amplitude in NH than in

10   SH, likely explained by the different land distribution in the two hemispheres and by the difference in the heat capacity of land and ocean. As known, in both hemispheres surface temperature follows solar heating and is dominated by the annual cycle, with a weak semiannual component (Peixoto and Oort, 1992). Moreover, the amplitude of the NH surface temperature annual cycle is roughly twice as strong as the SH and they are in phase opposition so that, on the global scale, the mean surface temperature has a weaker residual seasonal cycle (Covey et al., 2000). Also, to be noted is the phase opposition

15   between surface temperature and baroclinicity index, with the latter showing a semiannual modulation of the annual cycle (Figure 3 when compared with Figure 2). Such a modulation, which in SH is a signature of SAO phenomenon (van Loon, 1967; Meehl, 1991), is found also in NH.

As an example, the time series of surface temperature and baroclinicity from the 6 selected CMIP3 models are shown in Figure 4 for the common time section 1979–1999. For the sake of clarity, the time series of T2m and σ_{BI} are standardized

20   and plotted into the same graphs. As expected, there is an opposite phase relationship between baroclinicity and surface temperature; furthermore, as shown by the reanalysis data, there is evidence in model data of the semiannual oscillation in both hemispheres, suggesting the robustness of such a feature in the time series. A few outliers are found in baroclinicity records, likely related to anomalous values in air temperature data.

3.2 Spectral estimates

25   The power spectral density (PSD) estimates of ERAI mean baroclinicity and surface temperature, for the NH and SH midlatitudes, computed using the MTM method are shown in Figure 5 (p = 3, K = 5). Peaks are tested for significance at 95 % level relative to the null hypothesis of a red noise background estimated from the data.

As already suggested by Figure 2 and 3, in both surface temperature and baroclinicity spectra most power is at the annual frequency, leading to a peak that is statistically significant. A secondary harmonic lies at the semiannual frequency, which,

30   for the baroclinicity index, is statistically significant or marginally significant in both hemispheres (i.e., the red noise spectrum lies within the confidence interval of PSD estimate), while for surface temperature it is not in NH and marginally statistically significant in SH. This means that in NH midlatitudes surface temperature is dominated by the annual cycle modulated by a weaker semiannual periodicity embedded into the red noise background, suggesting a more regional nature

of the semiannual component. Since we are interested to investigate the relationship between surface temperature and baroclinicity annual/semiannual cycles, we selected ocean regions in NH midlatitudes where baroclinic eddies are known to be particularly active and requiring that also the semiannual component in T2m is present (statistically significant). Candidate regions of interest are: NH oceans, Pacific Ocean, and Atlantic Ocean, all in the latitude band 30–60°N. For these

5   regions, power spectra of baroclinicity index (not shown) are characterized by statistically significant annual and semiannual cycles, with the exception of the Atlantic Ocean where no semiannual harmonic is found. The power spectra estimates of surface temperature are shown in Figure 6: as can be noted, for the Pacific Ocean the red noise spectrum falls within the confidence interval of the PSD estimate. Hence, for NH, we decided to focus the subsequent analysis on this region.

Results of bivariate spectral analysis (coherency and phase spectra) are shown in Figure 7 for the reanalysis ERAI and in

10   Figures 8–9 for model outputs, respectively. According to the adopted convention, in case of a phase value between $0°$ and $180°$ surface temperature is leading with respect to baroclinicity, and vice versa in case of a phase value between $180°$ and $360°$.

Consistently with Figure 5 and 6, the coherency spectra between observed surface temperature and baroclinicity in NH and SH (Figures 7a and 7c) show peaks at the annual frequency very close to the level of 1 (total coherency), implying strong

15   correlation between the two time series. Similarly, at the semiannual frequency high coherency is found in both hemispheres. This finding provides evidence for the already mentioned SAO and, more importantly, confirms the relationship between the two variables at the semiannual periodicity also in NH Pacific Ocean.

For most frequencies, phase spectra (Figures 7b and 7d) depart from the condition of null phase. In particular, in the NH Pacific Ocean at the annual frequency, a phase shift of about $213°$ is found (i.e., about $30°$ with respect to the opposition of

20   phase), and about $258°$ at the semiannual one. In the SH, at the annual frequency a phase shift of about $214°$ is observed and at the semiannual frequency about $235°$, showing, in both cases, a delay of the mean surface temperature with respect to the baroclinicity index.

Results obtained for the annual frequency in NH Pacific Ocean and SH are consistent with the baroclinic activity at midlatitudes that is particularly intense during winter when the meridional temperature gradients are stronger than during

25   summer. The lag with respect to the perfect opposition of phase, observed in both NH and SH, which is of about 1 month in terms of time (Grinsted et al., 2004), is likely associated to the larger thermal inertia of the oceans when compared with land surfaces as it is for the NH Pacific Ocean and SH midlatitudes. This is supported by a comparative analysis of the annual component of the time series that shows for the NH midlatitudes (dominated by land continents) an almost full opposition of phase between surface temperature and baroclinicity, and for the ocean regions a shift of about 1 month with respect to the

30   phase opposition.

At the semiannual frequency, a phase shift of about $50°$ is observed in SH and about $80°$ in NH Pacific, with surface temperature delaying by about 1 month or more compared to the opposition of phase: results seem in agreement with the SAO phenomenon and may be indicative of the role of the semiannual variability in shaping eddy activity (an example is the midwinter suppression characterizing the North Pacific storm tracks). Also, the high values of coherency found at the

semiannual frequency suggest that, as it is in the SH, the contribution of such harmonic to the NH ocean variability is not negligible.

Bivariate spectral analysis is applied to CMIP3 model outputs by considering the common time section 1900–1999 and the same number of tapers as for the reanalysis ($K = 5$). The latter choice implied the same degrees of freedom and, hence, the

5   same confidence level estimate. Results are shown in Figures 8–9.

With regard to the coherence spectra (Figures 8a, 9a), at the annual and semiannual frequencies, all CMIP3 models show high values well above the confidence level threshold both in NH Pacific and SH, in agreement with ERAI. Phase spectra (Figures 8b, 9b), instead, show some discrepancies with the reanalysis and among models (Table 2). Generally, in both hemispheres, there is more uncertainty in the reproduction of the phase of the semiannual cycle than of the annual one. In

10   particular, while at the annual frequency almost all CMIP3 models reproduce quite well the opposition of phase with 1-month delay of surface temperature (exceptions are CGCM3.1 and ECHAM5/MPI-OM for NH Pacific and GFDL-CM2.1 for SH), at the semiannual frequency three (NH Pacific) and two (SH) out of six models display phase values within the reanalysis error intervals (see Table 2). However, it is worth noticing that no CMIP3 model reproduces the reanalysis values at both the annual and semiannual frequencies in the two hemispheres. Moreover, it emerges that larger errors characterize

15   phase estimates at the semiannual frequency when compared to those obtained for the annual one, likely due to the less power of the six-month peak as resulted from the power spectra (Figure 5, 6).

To better illustrate the discrepancy among models, the scatter plots of the relative phase between surface temperature and baroclinicity at the annual and semiannual frequency, for both NH and SH, are shown in Figure 10a, b, respectively, for ERAI (green) and CMIP3 (blue). On the same plots results obtained from CMIP5 are also displayed (red) for comparisons,

20   see also Table 2 for phase values. In performing the bivariate spectral analysis for CMIP5, the same time period used for CMIP3 has been considered (i.e., 1900–1999), with the exception of CanCM4 model that has a different time section (1961–1999). It clearly emerges that for CMIP3 while the uncertainty in the phase at the annual frequency is bounded between about $\pm 15^{o}$ around an average value of about 220°, phase estimates at the semiannual frequency span a wider range of values (from 240° to 360° in NH Pacific, from 120° to 300° in SH). Findings seem to suggest that there is no evidence of the

25   relationship between models' horizontal resolution and their performance. Furthermore, it is worth noting that for the semiannual frequency model errors are larger when compared with those obtained for the annual one (twice or more).

Results obtained for the most recent multi-model dataset CMIP5 show several improvements compared with CMIP3, especially for the semiannual frequency in NH: phase values span between about 220° and 300° (i.e., about 1 month phase shift) for NH Pacific, and between about 180° and 280° (i.e., about 2 months) for SH. Larger errors of model estimates allow

30   their overlap with the reanalysis error bars; the non-overlapping among some models errors also occurs, denoting a degree of uncertainty in model data also in CMIP5.

Although MIROC5 show improved results, at the stage of the present analysis, overall, it is not possible to determine whether model changes, involving for example the horizontal resolution, have a significant impact on the representation of the semiannual period variability.

Earth System
Dynamics

Discussions

EGU

4 Summary and conclusions

The annual and seasonal cycles in the time series of surface air temperature and baroclinicity are analyzed in both hemispheres using ERAI reanalysis data covering the period 1979–2015 and AOGCM outputs from CMIP3 and CMIP5 experiments of different record lengths.

5 The baroclinicity index time series is estimated through the tropospheric meridional temperature gradient (Eady maximum growth rate), which is computed as the difference between the poleward and equatorward edges midlatitude band (30°–60° for the NH and 30°–70° for the SH, respectively), and zonally and vertically averaged in each hemisphere, while surface temperature time series is obtained by zonally and meridionally averaging over the same latitude band.

The spectral analysis carried out applying the MTM method shows that annual and semiannual periodic components are the

10 dominating features in the reanalysis time series and model outputs. In particular, results show the occurrence of the semiannual oscillation in the zonally averaged baroclinic activity in both hemispheres. The presence of the semiannual peak in the NH baroclinicity may be considered a signature of the midwinter Pacific suppression as suggested by Nakamura et al. (1992), but further investigations are necessary.

The bivariate analysis of coherency and phase spectra between baroclinicity and surface temperature show discrepancies

15 between ERAI and model data, as well as among models, especially for the semiannual frequency. In particular, for ERAI it is found that:

   (i)   At the annual and semiannual frequencies, a very high coherency between the two selected variables is observed;

   (ii) At the annual frequency, in both hemispheres baroclinicity leads surface temperature of about 30° with respect

20   to the phase opposition;

   (iii) At the semiannual frequency, the relative phase is shifted by about 70° with respect to the opposite phase condition in NH Pacific and by about 55° in SH (i.e., about 1 month delay of surface temperature with respect baroclinicity).

For models outputs:

25 (iv) For what concerns the coherency spectra, at the annual and semiannual frequency, coherency is well represented by all models in both hemispheres and well exceeds the confidence level. Results for CMIP5 models are in agreement with those presented for CMIP3;

   (v)   At the annual frequency, phase estimates in both hemispheres are bounded between about $\pm15^o$ around an average value of 220° (i.e., about 1 month phase shift). At the semiannual frequency, model relative phases

30   between surface temperature and baroclinicity show wider dispersion in both hemispheres, denoting discrepancies among models and wider uncertainty in the estimates. Results for CMIP5 display improvements when compared with CMIP3 with a reduction of the discrepancy among models, especially in NH Pacific.

Larger errors found at the semiannual frequency make phase estimates of most models consistent with the reanalysis (i.e., they fall within the ERAI confidence interval) but discrepancies still occur especially in SH.

In performing the present analysis two assumptions have been made that might be considered restrictive with possible impacts on the obtained results. They are the vertical averaging, which has not been weighted for the mass of the atmosphere, and the choice of the monthly mean of daily means data. About the former, it has been observed that the discretization of the vertical pressure levels already accounts for that, while the impact of the latter choice has been verified against the results obtained using daily means with not statistically significant differences.

Furthermore, the choice of the maximum Eady growth rate as an index of baroclinicity has been considered suitable for the purpose of the present paper because it has been widely used in the international literature and, in the framework of zonally averaged atmosphere, the variability of the tropospheric static stability (unlike the static stability ratio between troposphere and stratosphere) has been found to have a secondary effect on baroclinic activity (Bordi et al., 2002; Fantini, 2004). It is worth noticing that the presence of a statistically significant semiannual peak in surface temperature spectral estimates, may suggest that the internal forcing exerted by baroclinic eddies play a role in modulating the annual cycle.

The six-month modulation of the baroclinicity index is somewhat not surprising, since the relationship between baroclinic activity and SAO has been widely investigated (e.g., Walland and Simmonds, 1999). It has been found that the SAO phenomenon is related to the half-yearly wave in the meridional temperature gradient at high southern latitudes that implies seasonal fluctuations of baroclinicity and surface pressure; moreover, the variation of the static stability during the year seems to modulate the efficiency of baroclinic conversion. Some evidences of a semiannual modulation have been found also in NH at regional scale (e.g., Wikle and Chen, 1996), suggesting a mechanism for the SAO in NH based on the east-west land-sea contrast, similarly to the north-south differential heating in SH proposed by van Loon (1967). However, to the best of our knowledge, it is the first time this oscillation has been found in the zonally averaged NH midlatitudes. It is left to a future study whether it is just the projection on the zonal average of regional scale processes or it is the signature of a global scale phenomenon.

Present findings contribute to better characterize the cyclic response of current global atmosphere-ocean models to the external solar forcing that is of particular interest for seasonal forecasts. The discrepancies emerged with reanalysis and among models, at least for the AOGCMs here considered, in properly reproducing the seasonal cycle of surface temperature and baroclinicity require further investigations. A larger set of models should be considered and the performance of a model ensemble against reanalysis should be assessed rather than that of a single model. In doing this, a simple metric for the seasonal cycle should be developed and tested (see for example Gleckler et al., 2008).

**Earth System
Dynamics**
Discussions

Open Access

EGU

5 **References**

Berrisford, P., Dee, D., Poli, P., Brugge, R., Fielding, K., Fuentes, M., Kallberg, P., Kobayashi, S., Uppala, S., and Simmons, A.: The ERA-Interim archive, version 2.0. ERA report series. 1. Technical Report. ECMWF pp23, 2011.

Blackmon, M. L., Wallace, J. M., Lau, N.-C., and Mullen, S. L.: An observational study of the Northern Hemisphere wintertime circulation. J. Atmos. Sci., 34, 1040–1053, 1977.

10 Bordi, I., Dell'Aquila, A., Speranza, A., and Sutera, A.: Formula for a baroclinic adjustment theory of climate, Tellus, 54A, 260–272, 2002.

Bye, J., Fraedrich, K., Schubert, S., and Zhu, X.: The Changing length of the warming period of the annual temperature cycle in the high latitudes under global warming, Atmosphere-Ocean, 51, 309–318, 2013.

Carnell, R.E., and Senior, C.A.: Changes in mid-latitude variability due to increasing greenhouse gases and sulphate
15 aerosols, Clim. Dyn., 14, 369–383, 1998.

Chang, E.K.M.: Midwinter suppression of the Pacific storm track activity as seen in aircraft observations, J. Atmos. Sci., 60, 1345–1358, 2003.

Charney, J.G.: The dynamics of long waves in a baroclinic westerly current, J. Meteorol., 4, 135–162, 1947.

Chen, G., Qian, C., and Zhang, C.: New insights into annual and semiannual cycles of sea surface pressure, Mon. Wea. Rev.,
20 140, 1347–1355, 2012.

Covey, C., Abe-Ouchi, A., Boer, G.J., Boville, B.A., Cubasch, U., and co-authors: The seasonal cycle in coupled ocean-atmosphere general circulation models, Clim. Dyn., 16, 775–787, 2000.

Dee, D. P., Uppala, S. M., Simmons, A. J., Berrisford, P., Poli, P., and co-authors: The ERA-Interim reanalysis: configuration and performance of the data assimilation system, Q. J. R. Meteorol. Soc., 137, 553–597, 2011.

25 Dell'Aquila, A., Ruti, P.M., Sutera, A.: Effects of the baroclinic adjustment on the tropopause in the NCEP-NCAR reanalysis, Clim. Dyn., 28, 325–332, 2007a.

Dell'Aquila, A., Ruti, P.M., Calmanti, S., Lucarini, V.: Southern Hemisphere midlatitude atmospheric variability of the NCEP-NCAR and ECMWF reanalyses, J. Geophys. Res., 112, D08106, doi:10.1029/2006JD007376, 2007b.

Donohoe, A., and Battisti, D.S.: The seasonal cycle of atmospheric heating and temperature, J. Climate, 26, 4962–4980,
30 2013.

Eady, E.T.: Long waves and cyclone waves, Tellus, 1, 33–52, 1949.

13

Earth System
Dynamics
Discussions

Emanuel, K.A., Fantini, M., and Thorpe, A.J.: Baroclinic instability in an environment of small stability to slantwise moist convection. Part I. Two-dimensional models, J. Atmos. Sci., 44, 1559–1573, 1987.

Geng, Q., and Sugi, M.: Possible changes of extratropical cyclone activity due to enhanced greenhouse gases and sulfate aerosols – Study with a high-resolution AGCM, J. Climate, 16, 2262– 2274, 2003.

5   Ghil, M., Allen, M.R., Dettinger, M.D., Ide, K., Kondrashov, D., Mann, M.E., Robertson, A.W., Saunders, A., Tian, Y., Varadi, F., and Yiou, P.: Advanced spectral methods for climatic time series, Rev. Geophys. 40, 1–41, 2002.

Gleckner, P.J., Taylor, K.E., and Doutriaux C.: Performance metrics for climate models, J. Geophys. Res., 113, D06104, doi:10.1029/2007JD008972, 2008.

Hansen, J., Johnson, D., Lacis, A., Lebedeff, S., Lee, P., Rind, D., and Russell, G.: Climate impact of increasing atmospheric

10   carbon dioxide, Science, 213, 957–966, 1981.

Hansen, J., and Labedeff, S.: Global trends of measured surface air temperature, J. Geophys. Res. 92, 13345–13372, 1987.

Held, I.M., and Larichev, V.D.: A scaling theory for horizontally homogeneous, baroclinically unstable flow on a beta plane, J. Atmos. Sci., 53, 946–952, 1996.

Heo, K.-Y., Ha, K.-J., and Lee, S.-S.: Warming of Western North Pacific Ocean and Energetics of Transient Eddy Activity,

15   Mon. Wea. Rev., 140, 2860–2873, 2012.

Holton, J.R.: An introduction to dynamic meteorology, 4th edition, Elsevier Academic Press, Oxford, UK, 2004.

Hoskins, B., and Valdes, P.: On the existence of storm-tracks, J. Atmos. Sci., 47, 1854–64, 1990.

Huybers, P., and Curry, W.: Links between annual, Milankovitch and continuum temperature variability, Nature, 441, 329– 332, 2006.

20   Kiehl, J., and Trenberth, E.K.: Earth's annual global mean energy budget, Bull. Amer. Meteor. Soc., 78, 197–208, 1997.

Kim, K.-Y., and North ,G.R.:Seasonal cycle and second-moment statistics of a simple coupled climate system, J. Geophys. Res., 97, 20437–20448, 1992.

Knutti, R., Meehl, G.A., Allen, M.R., and Stainforth, D.A.: Constraining climate sensitivity from the seasonal cycle in surface temperature, J. Climate, 19, 4224–4233, 2006.

25   Lindzen, R., and Farrell, B.: A simple approximate result for the maximum growth rate of baroclinic instabilities, J. Atmos. Sci., 37, 1648–54, 1980.

Lindzen, R.S., Kirtman, B., Kirk-Davidoff, D., and Schneider, E.K.: Seasonal surrogate for climate, J. Climate., 8, 1681– 1684, 1995.

Lorenz, E.N.: Available potential energy and the maintenance of the general circulation, Tellus, 7, 157–167, 1955.

30   Lorenz, E.N.: Forced and free variations of weather and climate, J. Atmos. Sci., 36, 1367–1376, 1979.

Lucarini, V., Calmanti, S., Dell'Aquila, A., Ruti, P.M., and Speranza, A.: Intercomparison of the northern hemisphere winter midlatitude atmospheric variability of the IPCC models, Clim. Dyn., 28, 829–849, 2007.

Meehl, G.A.: A reexamination of the mechanism of the semiannual oscillation in the southern hemisphere, J. Climate., 4, 911–926, 1991.

14

Earth System Dynamics
Discussions
Open Access

Meehl, G.A., Covey, C., Delworth, T., Latif, M., McAvaney, B., Mitchell, J., Stouffer, R., and Taylor, K.: The WCRP CMIP3 multi-model dataset: a new era in climate change research, Bull. Amer. Meteor. Soc., 88, 1383–1394, 2007.

Nakamura, H.: Midwinter suppression of baroclinic wave activity in the Pacific, J. Atmos. Sci., 49, 1629–1642, 1992.

Peixoto, J.P., and Oort, A.H.: Physics of Climate. Springer-Verlag, 520 pp., 1992.

5 Percival, D.B., and Walden, A.T.: Spectral Analysis for Physical Applications: Multitaper and Conventional Univariate Techniques. Cambridge: Cambridge University Press, 1993.

Poli, P., Dee, D., Berrisford, P., and Thépaut, J.-N.: Overview of satellite data assimilation in the ERA-INTERIM reanalysis, EUMETSAT P.57, ISBN 978-92-9110-089-7, 2010.

Simmons, A.J., and Hoskins, B.J.: Barotropic influences on the growth and decay of nonlinear baroclinic waves, J. Atmos.

10 Sci., 37, 1679–1684, 1980.

Stone, P.H., Ghan, S.J., Spiegel, D., and Rambaldi, S.: Short-term fluctuations in the eddy heat flux and baroclinic stability of the atmosphere, J. Atmos. Sci., 39:1734–1746, 1982.

Taylor, K.E., Stouffer, R.J., and Meehl, G.A.: An overview of the CMIP5 and the experiment design, Bull. Amer. Meteor. Soc., 93, 485–498, 2012.

15 Thomson, D.J.: Spectrum estimation and harmonic analysis. In Proceedings of the IEEE, Vol. 70, 1055–1096, 1982.

Trenberth, K.E.: What are the seasons?, Bull. Amer. Meteor. Soc., 64, 1276–1277, 1983.

Trenberth, K.E., and Stepaniak, D.P.: The flow of energy through the earth's cli- mate system, Quart. J. Roy. Meteor. Soc., 130, 2677–2701, 2004.

Van Loon, H.: The half-yearly oscillation in middle and high southern latitudes and the coreless winter, J. Atmos. Sci. 24,

20 472–486, 1967.

Von Storch, H., and Zwiers, W.: Statistical analysis in climate research. Cambridge University Press, Cambridge, ISBN:0521450713, 1999.

Yashayaev, I.M., and Zveryaev, I.I.: Climate of seasonal cycle in the north Pacific and north Atlantic oceans, Int. J. Climatol., 21, 401–417, 2001.

25 Walland, D., and Simmonds, I.: Baroclinicity, meridional temperature gradients, and the Southern Semiannual Oscillation, J. Climate, 12, 3376– 3382, 1999.

Wikle, C.K., and Chen, T.-C.: On the semiannual variation in the northern hemisphere extratropical height field, J. Climate, 9, 2250–2258, 1996.

Wu, Y., Ting, M., Seager, R., Huang, H.-P., and Cane, M.A.: Changes in storm tracks and energy transports in a warmer

30 climate simulated by the GFDL CM2.1 model, Clim. Dyn., 37, 53–72, 2011.

Earth System
Dynamics
Discussions

Table 1: Main characteristics of CMIP3 and CMIP5 models used for the analysis. Concerning the vertical resolution, "C" refers to cubed-sphered resolution, "Z" to σ-pressure hybrid coordinates.

| CMIP3	Model	Horizontal resolution (atmosphere)	Vertical resolution (atmosphere)	Horizontal resolution (ocean, in lon × lat)	Simulated years
High resolution	MIROC3.2	T106	σ56	0.28125°x0.1875°	1900–2000
Medium resolution	CGCM3.1	T63	Z31	1.40°x0.94°	1850–2000
	ECHAM5/MPI-OM	T63	H31	1.5°x1.5°	1860–2009
	FGOALS-g1.0	2.8°x2.8°	σ26	1.0°x1.0°	1850–1999
	GFDL-CM2.1	2.5°x2.0°	H24	1.0°x1.0°	1861–2000
Low resolution	INM-CM3.0	5°x4°	σ21	2.5°x2.0°	n/a
CMIP5					
High resolution	MIROC5		Z40	1.4°x0.5 (1.4°)	1850–2012
Medium resolution	CanCM4	T63	Z35	1.41°x0.94°	1961–2005
	MPI-ESM-MR	T63	Z47	1.5°x1.5°	1850–2005
	FGOALS-g2	2.8°x2.8° (equal area)	σ26	1.0°x1.0°	1850–2005
	GFDL-CM3	C48	Z48	1.0°x1.0°	1860–2005
	INM-CM4	2.0°x1.5°	σ21	1.0°x0.5°	1850–2005

5

Table 2: Phase values between surface temperature and baroclinicity computed using MTM method. Errors at 95 % confidence level are computed using Montecarlo simulations (2^{13}); phase values that fall within the confidence interval of the reanalysis ERAI are in bold.

	NH Pacific (30°–60°)		SH (30°–70°)	
	1 yr⁻¹	*2 yr⁻¹*	*1 yr⁻¹*	*2 yr⁻¹*
ERAI	213.1±3.3	258.0±11.2	214.5±6.9	235.4±10.8
CMIP3				
MIROC3.2	**214.1±2.3**	**253.6±14.8**	**209.8±3.5**	265.3±17.0
CGCM3.1	224.3±3.1	328.4±24.6	**215.8±2.7**	140.8±19.3
ECHAM5/MPI-OM	221.2±2.3	**274.7±17.0**	225.3±5.1	**245.5±21.9**
FGOALS-g1.0	**215.8±2.5**	338.0±19.4	**222.4±2.6**	281.4±16.3
GFDL-CM2.1	**216.7±2.7**	**264.1±19.8**	191.4±4.5	**244.0±17.6**
INM-CM3.0	**212.1±2.4**	303.8±26.6	**216.8±2.9**	268.7±18.3
CMIP5				
MIROC5	**217.8±3.7**	**274.5±16.0**	**209.6±10.0**	258.4±27.7
CanCM4	**216.7±2.9**	**244.4±10.8**	209.0±4.5	198.8±17.9
MPI-ESM-MR	226.3±3.5	**283.0±17.1**	224.6±8.0	**260.0±23.2**
FGOALs-g2	224.2±3.5	**253.7±15.7**	213.3±5.0	**244.5±25.7**
GFDL-CM3	**220.7±14.0**	**242.6±18.8**	**227.8±12.1**	**257.7±22.3**
INM-CM4	**215.8±3.7**	**266.2±18.0**	**223.7±3.7**	**218.3±20.0**

5

Earth System
Dynamics
Discussions
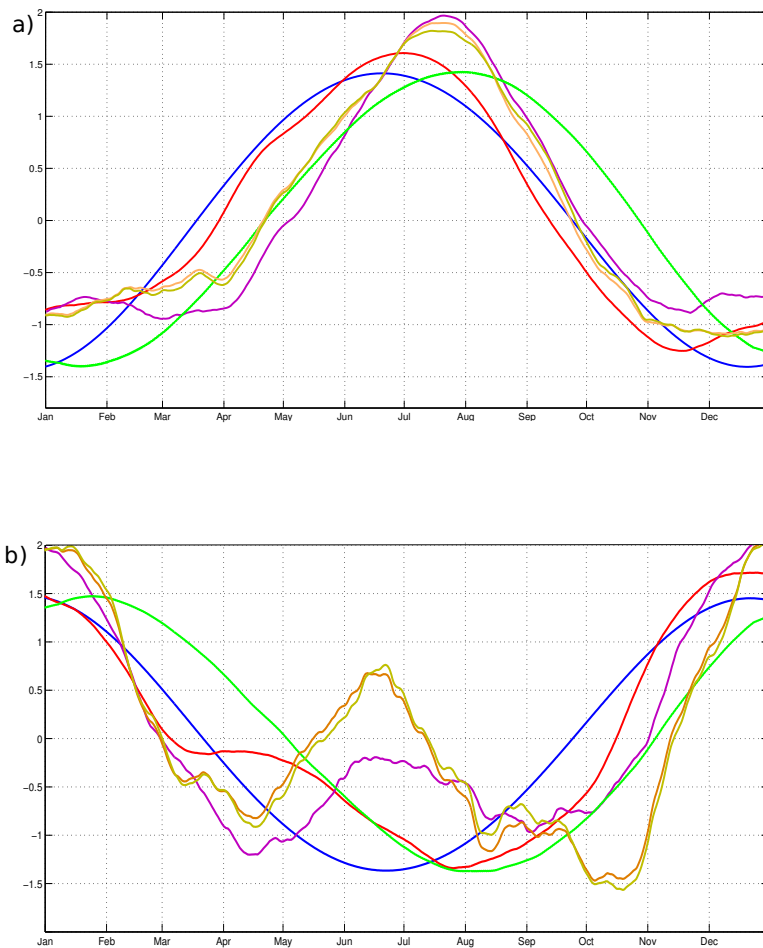
Figure 1: Mean annual cycles of midlatitude ERAI fields for the Northern (a) and Southern Hemispheres (b): surface temperature (T2m, green), baroclinicity index (σ_{BI}, purple), solar radiation at the top of the atmosphere (TOA, blue), mean sea level pressure variance (MSLP, red), meridional gradient of the geopotential field at 300 hPa and 500 hPa (yellow and khaki, respectively). Baroclinicity index, GPT, and MSLP variance cycles have been reversed so that their maxima occur in summer as for the other fields. Values are standardized.

Earth System
Dynamics
Discussions
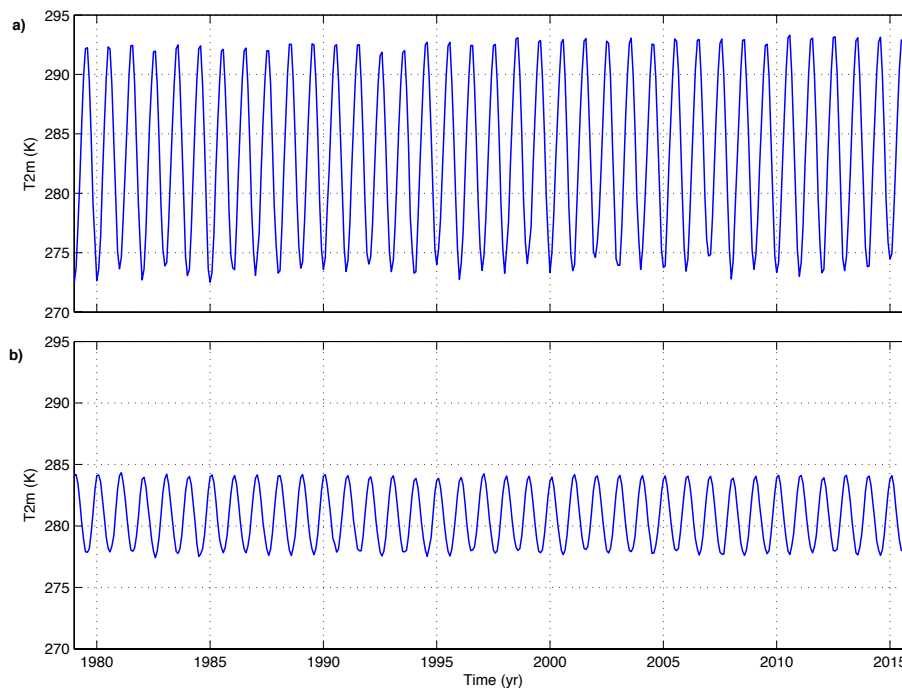
Figure 2: Monthly mean time series (1979–2015) of ERAI surface temperature (T2m) averaged over: a) the Northern Hemisphere (NH) and b) Southern Hemisphere (SH) midlatitudes (30–60°N and 30–70°S, respectively). Units are degree K.

Earth System
Dynamics
Discussions
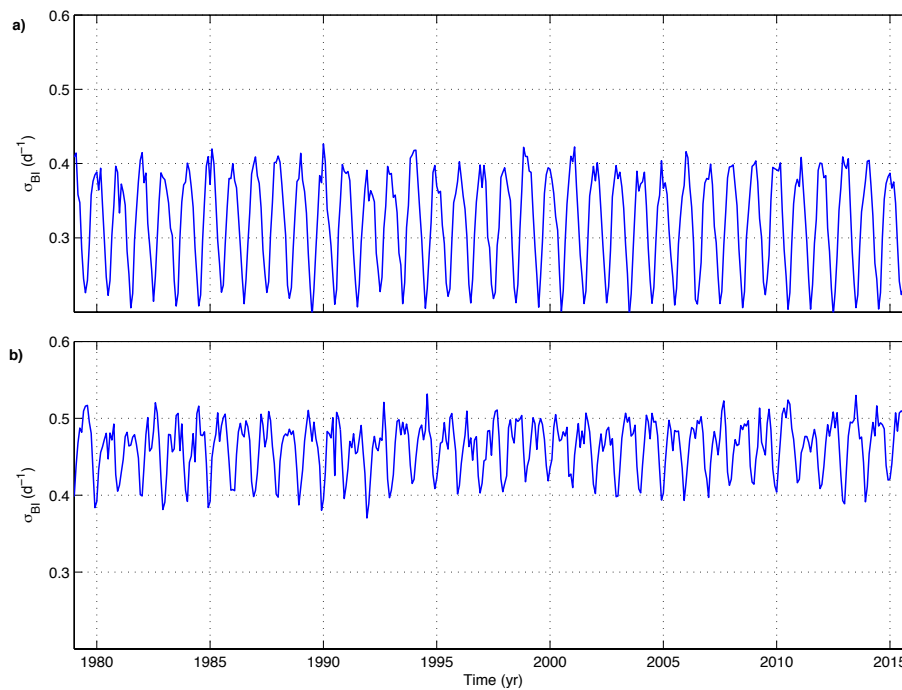
Figure 3: As in Figure 2 but for ERAI baroclinicity index (σ_{BI}). Units are d^{-1}.

Earth System
Dynamics
Discussions
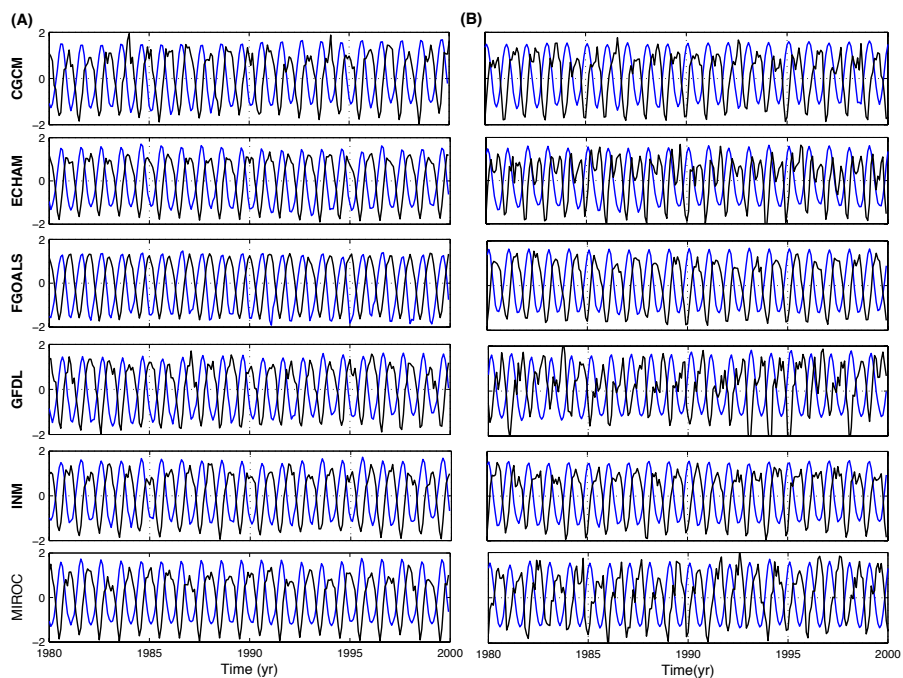
Figure 4: CMIP3: Time series of surface temperature (T2m, blue) and baroclinicity (σ_{BI}, black) for the 6 selected AOGCMs for the common time period 1979–1999. Time series are standardized.

Earth System
Dynamics
Discussions
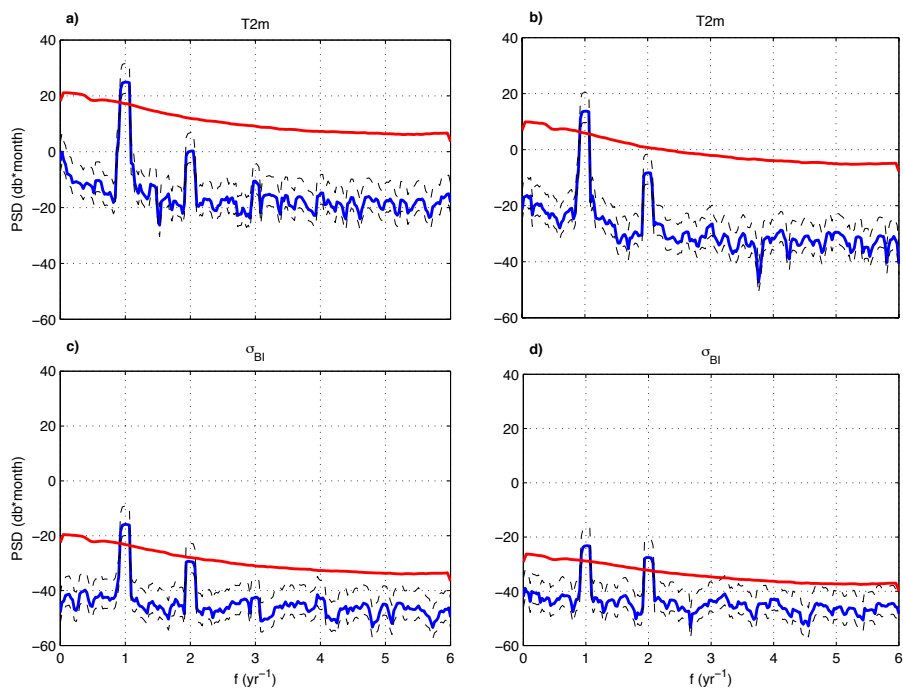
Figure 5: **Power spectral density (PSD) estimates of ERAI mean surface temperature (T2m) and baroclinicity (σ_{BI}), for the Northern (a, c) and Southern Hemispheres (b, d) midlatitudes, computed using the MTM method (parameters $p = 3$, $K = 5$). The 0.99 confidence intervals (dashed lines) are obtained by the Chi-squared distribution with 7 degrees of freedom; the red noise spectrum at 95 % level is in red. Frequency on the x-axis is in yr^{-1}.**
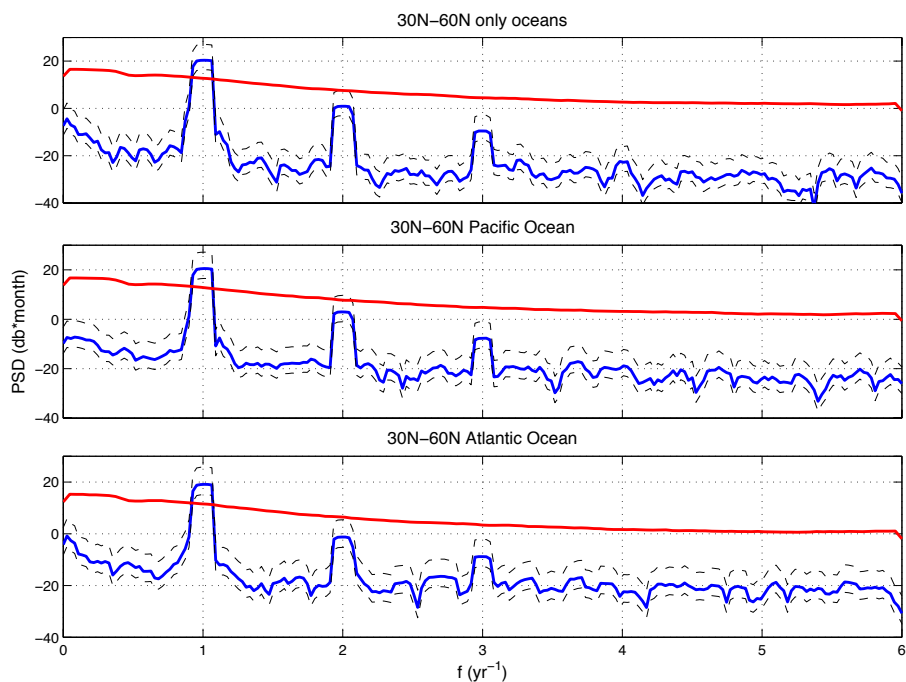
Earth System
Dynamics
Discussions

Figure 6: As in Figure 5 but for the following ocean regions: NH oceans (30°–60°N), Pacific Ocean (30°–60°N), Atlantic Ocean (30°–60°N).
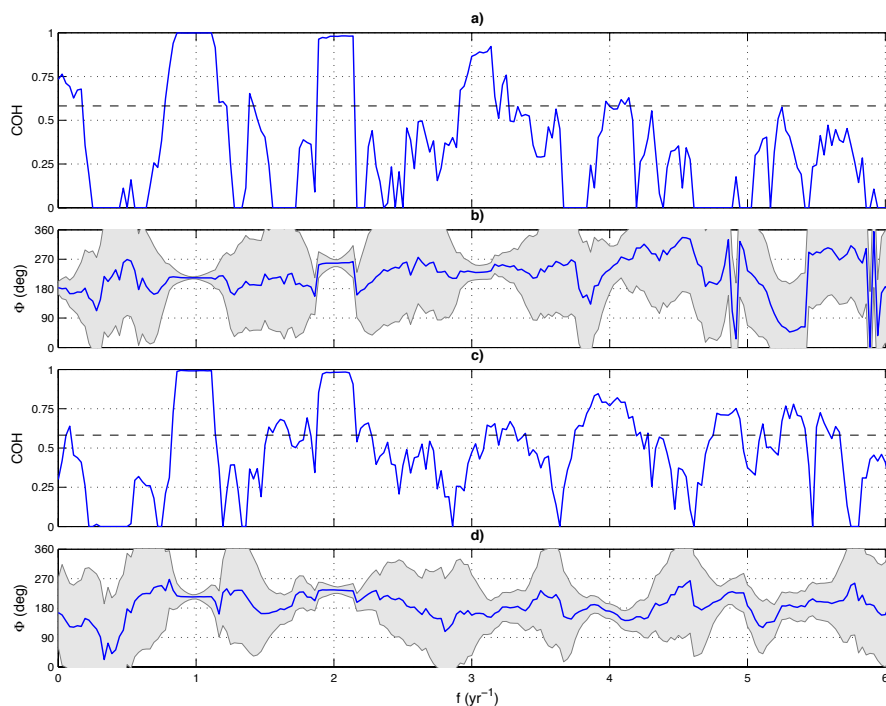
5

23

Figure 7: Bivariate spectral analysis (coherency and phase spectra) of ERAI surface temperature and baroclinicity for the period January 1979–September 2015: a)–b) NH midlatitude band 30°–60°N over the Pacific Ocean; c)–d) SH midlatitude band 30°–70°S. Dashed horizontal line in the coherency plot represents the 97.5% significance level; shaded areas in the phase plots represent the 95% level of significance obtained by means of 2^{13} Montecarlo simulations. Frequency on the x-axis is in yr^{-1}.
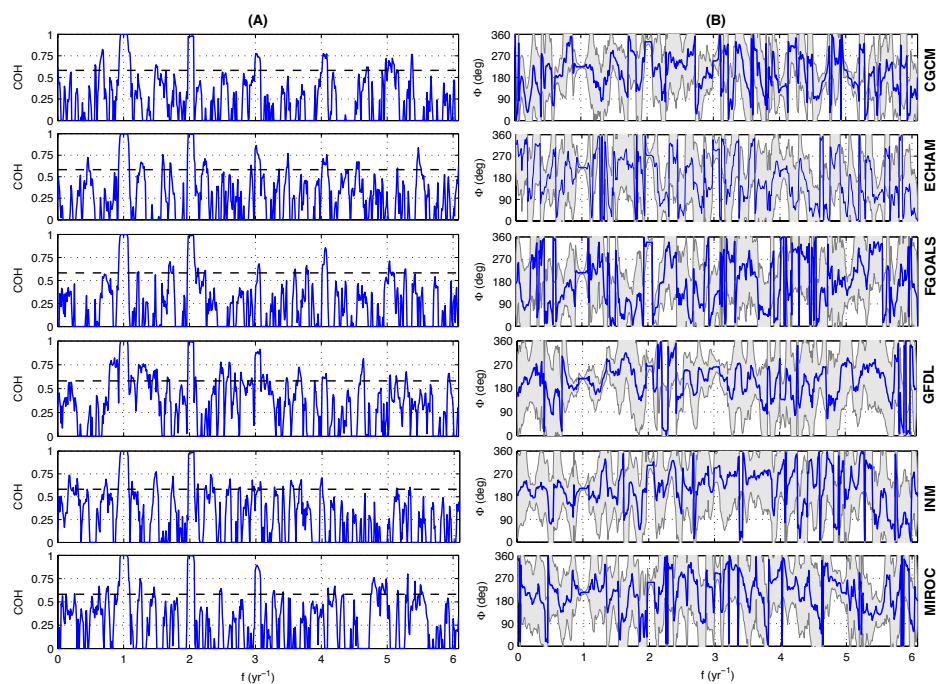
Earth System
Dynamics

Discussions

Figure 8: **Bivariate spectral analysis (coherence and phase spectra) of surface temperature and baroclinicity for the 6 selected CMIP3 models computed over the time period 1900–1999. Plots refer to the NH midlatitude band 30°–60°N over the Pacific Ocean. Dashed horizontal line represents the 97.5% significance level; shaded areas represent the 95% level of significance obtained by means of 2^{13} Montecarlo simulations.**
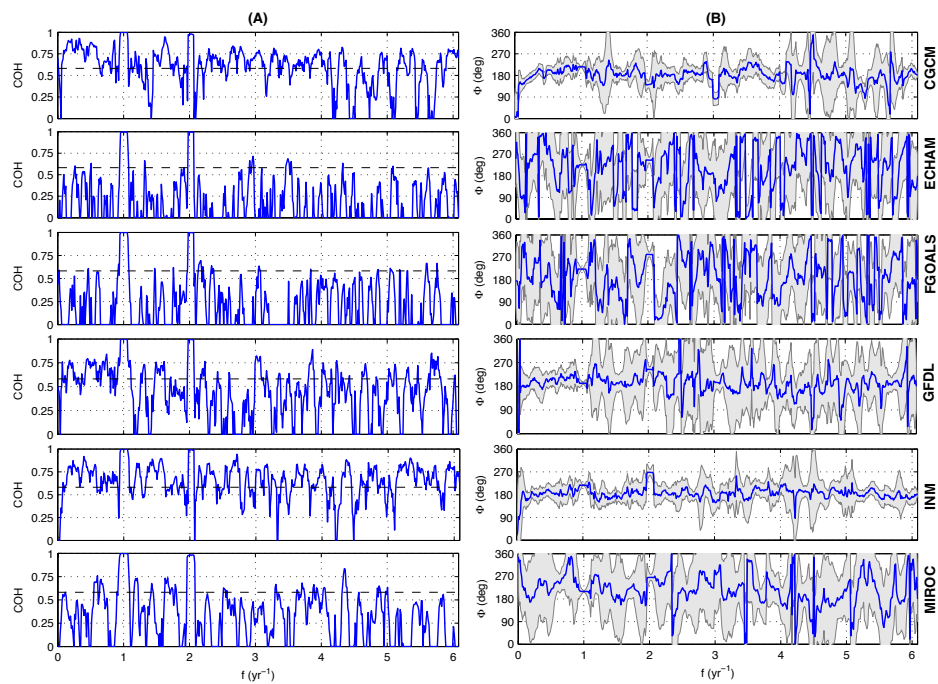
Earth System
Dynamics
Discussions

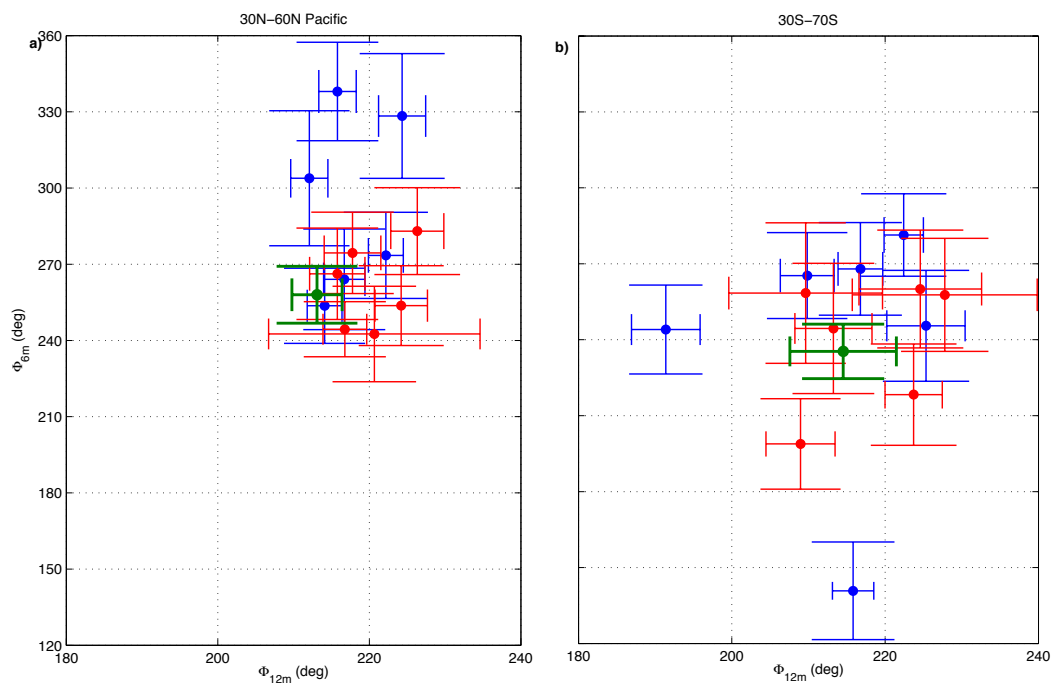Figure 9: As in Figure 8 but for the SH midlatitude band 30°–70°S.

Figure 10: Scatter plots of the relative phase between surface temperature and baroclinicity at the annual (Φ_{12m}) and semiannual (Φ_{6m}) frequency for: a) NH Pacific Ocean 30°–60°N, b) SH latitude band 30°–70°S. Estimates for ERAI reanalysis are in green, for CMPI3 and CMIP5 models are in blue and red, respectively. Error bars have been computed as in Figure 7.